An effective high order interpolation scheme in BIEMs for biharmonic boundary value problems

N. Mai-Duy* and R.I. Tanner

School of Aerospace, Mechanical and Mechatronic Engineering,

The University of Sydney, NSW 2006, Australia

Submitted to EABE, 13 September 2004; revised 21 December 2004

*Corresponding author: Telephone +61 2 9351 7151, Fax +61 2 9351 7060, E-mail nam.maiduy@aeromech.usyd.edu.au

Abstract This paper presents an effective high order boundary integral equation method (BIEM) for the solution of biharmonic equations. All boundary values including geometries are approximated by high order radial basis function networks (RBFNs) rather than the conventional low order Lagrange interpolation schemes. For a better quality of approximation, the networks representing the boundary values and their derivatives are constructed by using integration processes. Prior conversions of network weights into nodal variable values are employed in order to form a square system of equations. Numerical results show that the proposed BIEM attains a great improvement in solution accuracy, convergence rate and computational efficiency over the linear- and quadratic-BIEMs.

Keywords: indirect radial basis function networks; biharmonic equations; boundary integral equation methods.

1 Introduction

Many engineering problems, for example, viscous fluid flows and thin plate bending problems, are governed by biharmonic equations. Consequently, considerable effort has been devoted to the solution of biharmonic equations for many decades. Since exact analyses of such problems are usually very difficult, a variety of numerical methods have been developed.

The numerical analysis of biharmonic boundary value problems can be accomplished by a number of techniques: finite difference methods (FDMs), finite element methods (FEMs), boundary integral equation methods (BIEMs) and other methods. The BIEM has certain advantages over the domain type solution methods. For example, the system of equations obtained by BIEMs is much smaller than the system obtained by FDMs/FEMs. Furthermore, in solving homogeneous equations, it may require discretization only on the boundary. Once the boundary solutions are available, the solutions at any interior point can be obtained by direct evaluation.

Biharmonic boundary value problems have been studied extensively by BIEMs; a great number of publications are available in the literature (e.g. [1-12]). A boundary integral formulation for biharmonic boundary value problems consists of two equations in order to deal with four variables at each point on the boundary (two of them being unknown). A pair of boundary integral equations (BIEs) can be formed by a) the BIE of a biharmonic equation (standard BIE) and its normal derivative (hypersingular BIE) [2-4]; b) BIEs of two harmonic equations [5,6,10,12] or c) BIEs of a biharmonic equation and a harmonic equation [7,11]. The first formulation involves the complexity and high-order singularity of the kernel functions, leading to the great difficulty of numerical treatments while the last two formulations involve only weakly and CPV singular integrals, whose evaluations can be carried out by using logarithmic Gaussian quadrature/Telles transformation and constant potential hypothesis, respectively [13-15]. In contrast to the second formulation,

no volume integrals occur in the third formulation for solving homogeneous biharmonic equations.

In the context of function approximation/interpolation, the use of high order Lagrange polynomials does not guarantee to yield a better quality of approximation. High order schemes can induce some oscillations between nodal function values that may have no relation at all to the behaviour of the "true" function [16]. In the conventional BIEMs, low order Lagrange interpolation schemes such as constant, linear or quadratic elements are usually employed to represent the variations of boundary values. To obtain a high degree of accuracy, dense meshes are thus required in most cases. For the solution of boundary integral equations of the first kind, the use of large numbers of boundary elements can lead to ill-conditioned systems of algebraic equations.

Radial basis function networks (RBFNs) have become one of the main fields of research in numerical analysis [17]. The construction of an RBFN, in its most basic forms, consists of three layers: the input layer, the hidden layer and the output layer. There is a large class of RBFs whose interpolation matrices are always solvable provided that the data points are all different [18]. It has been proved that RBFNs have the property of universal approximation [19,20]. Another important point is the fact that the dimension of the hidden space is directly related to the capacity of the network to approximate a smooth input-output mapping [17]. According to the Cover theorem, the higher the dimension of the hidden space, the more accurate the approximation will be [21]. Theoretically, high order RBFNs can represent any continuous function to a prescribed degree of accuracy using relatively low numbers of data points. However, in practice, due to the lack of general mathematical theories for determining the optimal values of network parameters (e.g. the positions and the widths of RBFs), it is still difficult to achieve such a universal approximation. A function and its derivatives can be approximated by the direct RBFN (DRBFN) approach based on a differentiation process [22] or by the indirect RBFN (IRBFN) approach based on an integration process [23]. From an approximation

theoretic point of view, the approximating functions are expected to be much smoother through the integration process and therefore IRBFNs can have higher approximation power than DRBFNs. Numerical results have shown that the IRBFN approach performs better than the DRBFN approach and element-based approximation schemes in terms of accuracy and convergence rate [23].

For conventional BIE methods, the numerical procedure involves a subdivision of the boundary into a number of small elements. On each element, the geometry and the variables are assumed to have certain low order shapes such as constant, linear or quadratic ones. First order derivatives of the boundary quantities/the slope of approximate representations are discontinuous across elements. In the proposed BIE method, the boundary is subdivided into a number of large segments over each of which the geometry is smooth and the prescribed boundary conditions are of the same type. IRBFNs are employed to represent the variations of boundary quantities along these segments. They thus allow first and higher order derivatives to be continuous on large regions. Each segment is simply discretized by a set of discrete points rather than a set of intervals/elements. However, due to the fact that the construction of IRBFNs is based on an integration process, there are extra network weights (integration constants), leading to a non-square interpolation matrix.

It is different from previous works dealing with potential and viscous fluid flow problems that are governed by Poisson and the Navier-Stokes equations [24,25], prior conversions of the sets of network weights into the sets of nodal variable values are employed here in order to form a square system of equations that can be solved using Gaussian elimination. The linear- and quadratic-BIEMs are also considered to provide the basis for the assessment of the presently proposed IRBFN-BIEM. For the biharmonic Dirichlet problems of the first kind with non-smooth geometries and boundary conditions of complex shapes, it will be shown that the iterative decoupled approach has advantages over the usual non-iterative coupled approach with regard to the capability of preventing large fluctuations in the

computed boundary solutions. The proposed IRBFN-BIEM is found to be far superior to the conventional low order BIEMs for all numerical test cases.

The remainder of the paper is organized as follows. A brief review of the integral representation due to the coupled biharmonic and harmonic equations is given in section 2. Section 3 presents the indirect RBFN approach. The proposed IRBFN-BIEM is described in section 4 and then verified through a number of examples including some thin plate bending problems in section 5. Section 6 gives some concluding remarks.

2 Boundary integral equations for the biharmonic boundary value problem

Consider the biharmonic equation defined on a bounded domain Ω in the plane for a function $v(x, y)$,

$$\nabla^4 v = p(x, y), \tag{1}$$

where $p(x, y)$ is a known function of position. This equation is coupled with a set of prescribed boundary conditions to constitutive the biharmonic boundary value problem.

The biharmonic boundary value problems can be formulated in the form of boundary integral equations. A formulation due to the combined biharmonic and harmonic equations [7] is adopted here. By introducing a new variable $u = \nabla^2 v$, the boundary integral equations of two equations,

$$\nabla^2 u = p(x, y), \tag{2}$$

$$\nabla^4 v = p(x, y), \tag{3}$$

can be written as

$$C(P)u(P) + \int_\Gamma \frac{\partial G^H(P,Q)}{\partial n} u(Q) d\Gamma = \int_\Gamma G^H(P,Q) \frac{\partial u(Q)}{\partial n} d\Gamma$$
$$- \int_\Omega G^H(P,Q) p(Q) d\Omega, \tag{4}$$
$$C(P)v(P) + \int_\Gamma \frac{\partial G^H(P,Q)}{\partial n} v(Q) d\Gamma = \int_\Gamma G^H(P,Q) \frac{\partial v(Q)}{\partial n} d\Gamma$$
$$- \int_\Gamma \left(\frac{\partial G^B(P,Q)}{\partial n} u(Q) - G^B(P,Q) \frac{\partial u(Q)}{\partial n} \right) d\Gamma - \int_\Omega G^B(P,Q) p(Q) d\Omega, \tag{5}$$

where P is the source point, Q the field point, Γ the piecewise smooth boundary of Ω, $C(P)$ the free term coefficient which is 1 if P is an interior point, 1/2 if P is a point on the smooth boundary and $\frac{\theta}{2\pi}$ if P is a corner (θ the internal angle of the corner in radians), n the outward normal to the boundary, G^H and G^B the harmonic and biharmonic fundamental solutions, whose forms respectively are

$$G^H = \frac{1}{2\pi} \ln\left(\frac{1}{r}\right), \tag{6}$$
$$G^B = \frac{1}{8\pi} r^2 \left[\ln\left(\frac{1}{r}\right) + 1 \right], \tag{7}$$

in which $r = \|P - Q\|$. For viscous fluid flows, the variables v and u represent the streamfunction and vorticity, respectively while for thin plate bending problems, they are the deflection and "bending moment", respectively. The variable u has no physical meaning inside the plate domain, however it may be equal to the bending moment on the boundary.

3 Indirect RBFNs

In the present work, only two dimensional (2D) problems are considered. In view of the fact that the BIEM allows the reduction of the problem dimension by one, only

IRBFNs for a function and its derivatives in 1D domain need to be utilized. The ith order IRBFN, IRBFN-i, is defined as an RBFN approximation scheme in which the ith order derivative is decomposed into RBFs and then integrated i times. To represent the k order derivative, the order of IRBFNs should be equal to or greater than k. The effect of the order of IRBFNs on the accuracy of approximation has been investigated in [26]. Solving the governing integral equations (4)-(5) requires the approximation of functions: $v(s), \partial v(s)/\partial n, u(s)$ and $\partial u(s)/\partial n$, and two first derivatives: $\partial x(s)/\partial s$ and $\partial y(s)/\partial s$. The use of a second order, one order higher than the minimum requirement, seems to be sufficient and IRBFN-2 will be employed here

$$\frac{d^2 f(s)}{ds^2} = \sum_{i=1}^{m} w^{(i)} g^{(i)}(s), \tag{8}$$

$$\frac{df(s)}{ds} = \int \sum_{i=1}^{m} w^{(i)} g^{(i)}(s) ds + C_1 = \sum_{i=1}^{m+1} w^{(i)} H_{[1]}^{(i)}(s), \tag{9}$$

$$f(s) = \int \sum_{i=1}^{m+1} w^{(i)} H_{[1]}^{(i)} ds + C_2 = \sum_{i=1}^{m+2} w^{(i)} H_{[0]}^{(i)}(s), \tag{10}$$

where superscripts denote the elements of a set of neurons, m is the number of radial basis functions, $\{g^{(i)}\}_{i=1}^{m}$ the set of RBFs, $\{w^{(i)}\}_{i=1}^{m}$ the set of network weights to be found, $\{H_{[.]}^{(i)}\}_{i=1}^{m}$ new basis functions obtained from integrating the radial basis function g. For convenience of presentation, the integration constants which are unknowns here and their associated known basis functions (polynomial) on right hand sides of (9)-(10) are also denoted by the notations $w^{(i)}$ and $H_{[.]}^{(i)}$, respectively, but with $i > m$.

Among RBFs, multiquadrics (MQ) are ranked the best in terms of accuracy [27] and also possess exponential convergence with respect to the refinement of spatial discretization [28,29]. In the present work, the MQ is implemented and hence the basis functions g and

$H_{[.]}^{(i)}$ take the forms as

$$
\begin{aligned}
g^{(i)}(s) &= \sqrt{(s-c^{(i)})^2 + a^{(i)2}}, && (11)\\
H_{[1]}^{(i)}(s) &= \frac{(s-c^{(i)})}{2}A + \frac{a^{(i)2}}{2}B, && (12)\\
H_{[0]}^{(i)}(s) &= \left(\frac{-a^{(i)2}}{3} + \frac{(s-c^{(i)})^2}{6}\right)A + \frac{a^{(i)2}(s-c^{(i)})}{2}B, && (13)
\end{aligned}
$$

where $\{c^{(i)}\}_{i=1}^{m}$ is the set of RBF centres, $\{a^{(i)}\}_{i=1}^{m}$ the set of RBF widths, $A = \sqrt{(s-c^{(i)})^2 + a^{(i)2}}$ and $B = \ln\left((s-c^{(i)}) + \sqrt{(s-c^{(i)})^2 + a^{(i)2}}\right)$. To make the training process simple, the centres and widths of RBFs are chosen in advance. For the former, the set of centres is chosen to be the same as the set of collocation points, i.e. $\{c^{(i)}\}_{i=1}^{m} \equiv \{s^{(i)}\}_{i=1}^{n}$ with $n = m$, while for the latter, the following relation is used

$$a^{(i)} = \beta d^{(i)}, \tag{14}$$

where β is a positive scalar and $d^{(i)}$ is the minimum of distances from the ith center to its neighbours.

In the present study, the set of network weights $\{w^{(i)}\}_{i=1}^{m+2}$ is converted into the set of function values $\{f(s^{(i)})\}_{i=1}^{n}$ in order to form a square system of equations that can be solved by Gaussian elimination. The process is as follows. The evaluation of (10) at the set of collocation points $\{s^{(i)}\}_{i=1}^{n}$ results in

$$
\begin{pmatrix} f(s^{(1)}) \\ f(s^{(2)}) \\ \vdots \\ f(s^{(n)}) \end{pmatrix} = \begin{bmatrix} H_{[0]}^{(1)}(s^{(1)}) & \cdots & H_{[0]}^{(m)}(s^{(1)}) & s^{(1)} & 1 \\ H_{[0]}^{(1)}(s^{(2)}) & \cdots & H_{[0]}^{(m)}(s^{(2)}) & s^{(2)} & 1 \\ & \cdots & & & \\ H_{[0]}^{(1)}(s^{(n)}) & \cdots & H_{[0]}^{(m)}(s^{(n)}) & s^{(n)} & 1 \end{bmatrix} \begin{pmatrix} w^{(1)} \\ w^{(2)} \\ \vdots \\ w^{(m+2)} \end{pmatrix}. \tag{15}
$$

The obtained system (15) for the unknown vector of network weights can be solved using

general linear least squares

$$\begin{pmatrix} w^{(1)} \\ w^{(2)} \\ \vdots \\ w^{(m+2)} \end{pmatrix} = \begin{bmatrix} H_{[0]}^{(1)}(s^{(1)}) & \cdots & H_{[0]}^{(m)}(s^{(1)}) & s^{(1)} & 1 \\ H_{[0]}^{(1)}(s^{(2)}) & \cdots & H_{[0]}^{(m)}(s^{(2)}) & s^{(2)} & 1 \\ & \cdots & & & \\ H_{[0]}^{(1)}(s^{(n)}) & \cdots & H_{[0]}^{(m)}(s^{(n)}) & s^{(n)} & 1 \end{bmatrix}^{-1} \begin{pmatrix} f(s^{(1)}) \\ f(s^{(2)}) \\ \vdots \\ f(s^{(n)}) \end{pmatrix}, \tag{16}$$

or

$$\mathbf{w} = \mathbf{H}_{[\mathbf{0}]}^{-1}\mathbf{f}, \tag{17}$$

where $\mathbf{H}_{[\mathbf{0}]}^{-1}$ is the Moore-Penrose pseudoinverse and the dimensions of $\mathbf{w}$, $\mathbf{H}_{[\mathbf{0}]}^{-1}$ and $\mathbf{f}$ are $(m+2)\times 1$, $(m+2)\times n$ and $n\times 1$, respectively. As can be seen from (17), the network weights are expressed in terms of the function values $\{f^{(i)}\}_{i=1}^{n}$. By substituting (17) into (8)-(10), the function f and its derivatives at an arbitrary point s will be computed by

$$f(s) = \begin{bmatrix} H_{[0]}^{(1)}(s) & \cdots & H_{[0]}^{(m)}(s) & s & 1 \end{bmatrix} \mathbf{H}_{[\mathbf{0}]}^{-1} \begin{bmatrix} f^{(1)} f^{(2)} & \cdots f^{(n)} \end{bmatrix}^T, \tag{18}$$

$$\frac{df(s)}{ds} = \begin{bmatrix} H_{[1]}^{(1)}(s) & \cdots & H_{[1]}^{(m)}(s) & 1 & 0 \end{bmatrix} \mathbf{H}_{[\mathbf{0}]}^{-1} \begin{bmatrix} f^{(1)} f^{(2)} & \cdots f^{(n)} \end{bmatrix}^T, \tag{19}$$

$$\frac{d^2f(s)}{ds^2} = \begin{bmatrix} g^{(1)}(s) & \cdots & g^{(m)}(s) & 0 & 0 \end{bmatrix} \mathbf{H}_{[\mathbf{0}]}^{-1} \begin{bmatrix} f^{(1)} f^{(2)} & \cdots f^{(n)} \end{bmatrix}^T. \tag{20}$$

Since all basis functions in (18)-(20) are available in analytic forms, the present indirect RBFN formulation is truly meshless.

4 The IRBFN-BIEM algorithm

The boundary integral equations (4)-(5) governing biharmonic boundary value problems involve weakly and CPV singular integrals. In the present work, the former is evaluated by Telles quadratic transformation [15] while the latter is treated using the non-CPV-singular form of BIEs [30]. Equations (4)-(5) without the CPV singular integrals can be

written as

$$\int_{\Gamma} \frac{\partial G^H(P,Q)}{\partial n} \left(u(Q) - u(P)\right) d\Gamma = \int_{\Gamma} G^H(P,Q) \frac{\partial u(Q)}{\partial n} d\Gamma,$$
$$- \int_{\Omega} G^H(P,Q) p(Q) d\Omega, \tag{21}$$
$$\int_{\Gamma} \frac{\partial G^H(P,Q)}{\partial n} \left(v(Q) - v(P)\right) d\Gamma = \int_{\Gamma} G^H(P,Q) \frac{\partial v(Q)}{\partial n} d\Gamma$$
$$- \int_{\Gamma} \left(\frac{\partial G^B(P,Q)}{\partial n} u(Q) - G^B(P,Q) \frac{\partial u(Q)}{\partial n} \right) d\Gamma - \int_{\Omega} G^B(P,Q) p(Q) d\Omega. \tag{22}$$

The kernels $G^B(P,Q)$ and $\frac{\partial G^B(P,Q)}{\partial n}$ have no singularities; their integrals can be evaluated by using appropriate Gaussian quadrature formulae.

In the case of non-homogeneous equations, a function $p(x,y)$ generates the volume integrals. Since the function p is known, these volume integrals do not introduce any new unknowns. Several techniques have been developed for the evaluation of volume integrals, including cell integration approach, particular solution technique [31], multiple reciprocity method (MRM) [32] and dual reciprocity method (DRM) [33]. The present study is concerned with the enhancement of evaluating boundary integrals by using an effective interpolation scheme based on IRBFNs. For convenience, all volume integrals in the work presented here are converted into the boundary integrals with the help of the MRM,

$$\int_{\Omega} G^{[i]} f^{[i]} d\Omega = \sum_{j=i}^{\infty} \int_{\Gamma} \left(\frac{\partial G^{[j+1]}}{\partial n} f^{[j]} - G^{[j+1]} \frac{\partial f^{[j]}}{\partial n} \right) d\Gamma, \tag{23}$$

where the index i indicates a volume integral which occurs in the boundary integral equation, $f^{[j+1]}(x,y) = \nabla^2 f^{[j]}(x,y)$, and $G^{[j+1]}$ and $\partial G^{[j+1]}/\partial n$ are the $(j+1)$th order

fundamental solutions to the potential problems, whose forms for 2D problems are

$$
\begin{aligned}
G^{[j+1]} &= \frac{1}{2\pi} r^{2(j+1)} (A_{j+1} \ln \frac{1}{r} + B_{j+1}), && (24)\\
\frac{\partial G^{[j+1]}}{\partial n} &= \frac{1}{2\pi} r^{2(j+1)-1} \left[\left(2(j+1) \ln \frac{1}{r} - 1 \right) A_{j+1} + 2(j+1) B_{j+1} \right] \frac{\partial r}{\partial n}, && (25)\\
A_{j+1} &= \frac{A_j}{4(j+1)^2}, && (26)\\
B_{j+1} &= \frac{1}{4(j+1)^2} \left(\frac{A_j}{j+1} + B_j \right), && (27)\\
A_0 &= 1, \quad B_0 = 0, && (28)
\end{aligned}
$$

where $j = 0, 1, 2, \cdots$.

- For a volume integral in (21): $i = 0$, $j \geq 0$

$$
\begin{aligned}
&j = 0, G^{[0]} = G^H, f^{[0]} = p,\\
&j = 1, G^{[1]} = G^B, f^{[1]} = \nabla^2 p, \cdots,
\end{aligned}
$$

- For a volume integral in (22): $i = 1$, $j \geq 1$

$$
j = 1, G^{[1]} = G^B, f^{[1]} = p, \cdots .
$$

The procedural flow chart is summarized as follows

- Divide the boundary into a number of segments over each of which the boundary is required to be smooth and to have the same type of prescribed boundary conditions. Clearly, the size of segments in the proposed method can be chosen to be much larger than the size of elements in conventional BIEMs. As a result, the IRBFN approximation scheme allows first and higher order derivatives of the boundary quantities to be continuous on larger regions than the case of using constant, linear and quadratic elements. Furthermore, each segment here is simply represented by

a number of discrete points, leading to an easy process of numerical modelling. The boundary integrals in (21)-(22) are replaced by the summations of integrals corresponding to a series of segments;

- Approximate all boundary values including geometries on each segment by IRBFNs, e.g. for the variables

$$
\begin{aligned}
v(s) &= \left[\begin{array}{cccccc} H_{[0]}^{(1)}(s) & \cdots & H_{[0]}^{(m)}(s) & s & 1 \end{array} \right] \mathbf{H}_{[\mathbf{0}]}^{-1} \left[\begin{array}{cccc} v^{(1)} & v^{(2)} & \cdots & v^{(n)} \end{array} \right]^T, \\
\frac{\partial v(s)}{\partial n} &= \left[\begin{array}{cccccc} H_{[0]}^{(1)}(s) & \cdots & H_{[0]}^{(m)}(s) & s & 1 \end{array} \right] \mathbf{H}_{[\mathbf{0}]}^{-1} \left[\begin{array}{cccc} \frac{\partial v^{(1)}}{\partial n} & \frac{\partial v^{(2)}}{\partial n} & \cdots & \frac{\partial v^{(n)}}{\partial n} \end{array} \right]^T, \\
u(s) &= \left[\begin{array}{cccccc} H_{[0]}^{(1)}(s) & \cdots & H_{[0]}^{(m)}(s) & s & 1 \end{array} \right] \mathbf{H}_{[\mathbf{0}]}^{-1} \left[\begin{array}{cccc} u^{(1)} & u^{(2)} & \cdots & u^{(n)} \end{array} \right]^T, \\
\frac{\partial u(s)}{\partial n} &= \left[\begin{array}{cccccc} H_{[0]}^{(1)}(s) & \cdots & H_{[0]}^{(m)}(s) & s & 1 \end{array} \right] \mathbf{H}_{[\mathbf{0}]}^{-1} \left[\begin{array}{cccc} \frac{\partial u^{(1)}}{\partial n} & \frac{\partial u^{(2)}}{\partial n} & \cdots & \frac{\partial u^{(n)}}{\partial n} \end{array} \right]^T,
\end{aligned}
$$

and for the geometry

$$
\begin{aligned}
x(s) &= \left[\begin{array}{cccccc} H_{[0]}^{(1)}(s) & \cdots & H_{[0]}^{(m)}(s) & s & 1 \end{array} \right] \mathbf{H}_{[\mathbf{0}]}^{-1} \left[\begin{array}{cccc} x^{(1)} & x^{(2)} & \cdots & x^{(n)} \end{array} \right]^T, \\
y(s) &= \left[\begin{array}{cccccc} H_{[0]}^{(1)}(s) & \cdots & H_{[0]}^{(m)}(s) & s & 1 \end{array} \right] \mathbf{H}_{[\mathbf{0}]}^{-1} \left[\begin{array}{cccc} y^{(1)} & y^{(2)} & \cdots & y^{(n)} \end{array} \right]^T, \\
\frac{\partial x(s)}{\partial s} &= \left[\begin{array}{cccccc} H_{[1]}^{(1)}(s) & \cdots & H_{[1]}^{(m)}(s) & 1 & 0 \end{array} \right] \mathbf{H}_{[\mathbf{0}]}^{-1} \left[\begin{array}{cccc} x^{(1)} & x^{(2)} & \cdots & x^{(n)} \end{array} \right]^T, \\
\frac{\partial y(s)}{\partial s} &= \left[\begin{array}{cccccc} H_{[1]}^{(1)}(s) & \cdots & H_{[1]}^{(m)}(s) & 1 & 0 \end{array} \right] \mathbf{H}_{[\mathbf{0}]}^{-1} \left[\begin{array}{cccc} y^{(1)} & y^{(2)} & \cdots & y^{(n)} \end{array} \right]^T, \\
d\Gamma &= \sqrt{\left(\frac{\partial x}{\partial s} \right)^2 + \left(\frac{\partial y}{\partial s} \right)^2} ds,
\end{aligned}
$$

where s is the independent variable, and $\{v^{(i)}\}_{i=1}^n$, $\{\partial v^{(i)}/\partial n\}_{i=1}^n$, $\{u^{(i)}\}_{i=1}^n$, $\{\partial u^{(i)}/\partial n\}_{i=1}^n$, $\{x^{(i)}\}_{i=1}^n$ and $\{y^{(i)}\}_{i=1}^n$ are the sets of nodal variable values.

- Substitute the IRBFNs representing the boundary values into the boundary integral equations (21)-(22);

- Discretize the system by collocating BIEs at the boundary nodes and then carry

out numerical integrations in the local coordinate system;

- Solve the obtained system of algebraic equations using the coupled or decoupled approach, depending on the geometry and the type of boundary conditions as will be discussed in the following section;
- Evaluate the solution at selected interior points;
- Output the results.

5 Numerical examples

A number of examples are presented in this section for the purpose of demonstrating the effectiveness of the proposed method. The linear- and quadratic-BIEMs are also considered to provide the basis for the assessment of the IRBFN-BIEM. To describe the multi-valued normal derivatives $\partial v/\partial n$ and $\partial u/\partial n$ at a corner, two extreme points on each segment are shifted into the segment by the amount of a quarter of the length between two nodes for the IRBFN-BIEM code while discontinuous elements are employed for the linear- and quadratic-BIEM codes.

In the following test cases, the width of the ith RBF is simply chosen to be the minimum distance from the ith centre to neighbouring centres ($a^{(i)} = \beta d^{(i)} = d^{(i)}$). The accuracy of numerical solution produced by an approximation scheme is measured via the norm of relative errors of the solution as follows

$$N_e = \sqrt{\frac{\sum_{i=1}^{n_t} \left[f_0((x,y)^{(i)}) - f((x,y)^{(i)})\right]^2}{\sum_{i=1}^{n_t} f_0((x,y)^{(i)})^2}}, \tag{29}$$

where n_t is the number of test points, $(x,y)^{(i)}$ is the ith test point, f and f_0 are the calculated and exact solutions, respectively. Another important measure is the convergence

rate of the solution with respect to the refinement of spatial discretization

$$N_e(\bar{s}) \approx \gamma \bar{s}^{\alpha} = O(\bar{s}^{\alpha}) \tag{30}$$

in which $\bar{s}$ is the average centre spacing, and α and γ are the exponential model's parameters. Given a set of observations, these parameters can be found by general linear least squares.

In the present study, of particular interest are the prescribed boundary conditions of the form: $\{v; \partial^2 v/\partial n^2\}$ (the second biharmonic Dirichlet problem) and $\{v; \partial v/\partial n\}$ (the first biharmonic Dirichlet problem).

5.1 Boundary conditions given in terms of v and u (BC1)

In this case, each integral equation has its own boundary condition. The integral equations (21) and (22) are weakly coupled and hence they can be solved separately. An approximation to the variable $\partial u/\partial n$ is first determined by solving (21). The obtained solution is then utilized to solve (22) for the variable $\partial v/\partial n$.

5.1.1 Example 1: a benchmark test problem (BTP), BC1, rectangular domain

Consider the homogeneous biharmonic equation $\nabla^4 v = 0$; the exact solutions are given by

$$
\begin{aligned}
v &= \frac{1}{2}x\left(\sin x\cosh y - \cos x\sinh y\right), && (31)\\
\frac{\partial v}{\partial x} &= \frac{1}{2}\left(\sin x\cosh y - \cos x\sinh y\right) + \frac{1}{2}x\left(\cos x\cosh y + \sin x\sinh y\right), && (32)\\
\frac{\partial v}{\partial y} &= \frac{1}{2}x\left(\sin x\sinh y - \cos x\cosh y\right), && (33)\\
\frac{\partial v}{\partial n} &= \frac{\partial v}{\partial x}n_x + \frac{\partial v}{\partial x}n_y, && (34)\\
u &= \cos x\cosh y + \sin x\sinh y, && (35)\\
\frac{\partial u}{\partial x} &= \cos x\sinh y - \sin x\cosh y, && (36)\\
\frac{\partial u}{\partial y} &= \sin x\cosh y + \cos x\sinh y, && (37)\\
\frac{\partial u}{\partial n} &= \frac{\partial u}{\partial x}n_x + \frac{\partial u}{\partial x}n_y, && (38)
\end{aligned}
$$

where n_x and n_y denote two components of the outward normal unit vector in the x and y directions, respectively. This is a typical benchmark test problem (BTP), where all boundary data are nonzero [9].

A unit square domain is considered. The boundary is divided into four segments corresponding to four edges of the domain. Ten uniform discretizations of the boundary, namely $3\times 4, 5\times 4, \cdots, 21\times 4$ (number of nodes per segment $\times$ number of segments), are employed to study this problem. A set of 26×4 test points is used to compute the error norm N_e of the boundary solutions for all discretizations. The obtained results are displayed in Figure 1. Results by the linear- and quadratic-BIEMs are also included for comparison. The proposed method yields the most accurate results, followed by the quadratic-BIEM and linear-BIEM. At the first four coarse discretizations, the conver-

gence rates are $O(\bar{s}^{1.76})$, $O(\bar{s}^{2.70})$ and $O(\bar{s}^{3.48})$ for linear-, quadratic- and IRBFN-BIEMs, respectively.

5.1.2 Example 2: a simply supported square plate with a concentrated load at the centre

For this problem, the volume integrals, which are generated by the concentrated force $F = 1$ at the centre O, are easily evaluated as follows

$$\int_\Omega G^H(P,Q)p(Q)d\Omega = \int_\Omega G^H(P,Q)\left(F(O)\delta(O,Q)\right)d\Omega = F(O)G^H(P,O), \quad (39)$$

$$\int_\Omega G^B(P,Q)p(Q)d\Omega = \int_\Omega G^B(P,Q)\left(F(O)\delta(O,Q)\right)d\Omega = F(O)G^B(P,O). \quad (40)$$

The analytical solution of this problem can be found in Timoshenko and Woinowsky-Krieger [34]. Three uniform boundary discretizations, namely $3\times4, 5\times4$ and 7×4, and a test set of 30×4 nodes are employed to study mesh convergence. The linear-, quadratic- and IRBFN-BIEMs yield the convergence rates of $O(\bar{s}^{1.92})$, $O(\bar{s}^{2.05})$ and $O(\bar{s}^{4.97})$, and the error norms at the finest discretization of 0.012, 0.0052 and $2.42e-4$, respectively.

5.1.3 Example 3: simply supported square plates under a uniform load and hydrostatic pressure

A simply supported plate of dimension $[0,200]\times[0,200]$ cm^2 with a uniform load q is considered here. Analytical solutions are available for this problem [34]. The parameters of the problem are

$$E = 2.1\times10^6\text{kg/cm}^2,\ q = 0.5\text{kg/cm}^2,$$
$$h = 10\text{cm},\ \nu = 0.3, D = Eh^3/[12(1-\nu^2)],$$

where E is the Young's modulus, ν the Poisson's ratio, h the plate thickness and D the flexural rigidity. The source function becomes

$$p(x, y) = q/D = \text{constant}.$$

For this simple form of the source function, the series in (23) becomes a finite summation. With the help of the MRM, the volume integrals in (21)-(22) are transformed into the following boundary integrals

$$\int_\Omega G^H p d\Omega = \int_\Omega G^{[0]} p d\Omega = \int_\Gamma \left(\frac{\partial G^{[1]}}{\partial n} p - G^{[1]} \frac{\partial p}{\partial n} \right) d\Gamma = p \int_\Gamma \frac{\partial G^{[1]}}{\partial n} d\Gamma, \tag{41}$$

$$\int_\Omega G^B p d\Omega = \int_\Omega G^{[1]} p d\Omega = \int_\Gamma \left(\frac{\partial G^{[2]}}{\partial n} p - G^{[2]} \frac{\partial p}{\partial n} \right) d\Gamma = p \int_\Gamma \frac{\partial G^{[2]}}{\partial n} d\Gamma. \tag{42}$$

The boundary is divided into 4 segments corresponding to four edges of the domain. Table 1 summarizes the results on the boundary obtained by the proposed method and the linear-BIEM [6]. With the same boundary discretization of 9×4, the proposed method yields more accurate results than the linear-BIEM.

To further demonstrate the effectiveness of the proposed method for the second biharmonic Dirichlet problems, a simply supported unit square plate under hydrostatic pressure is considered here. Using only coarse discretizations, accurate results are obtained. For example, with 5×4 boundary nodes, the dimenionless deflections along the horizontal centreline are $u(0.25, 0.5) = 0.00131$, $u(0.5, 0.5) = 0.00203$, $u(0.6, 0.5) = 0.00202$ and $u(0.75, 0.5) = 0.00162$; they are in good agreement with the values reported in [34]: 0.00131, 0.00203, 0.00201 and 0.00162, respectively.

5.2 Boundary conditions given in terms of v and $\partial v/\partial n$ (BC2)

In this case, all boundary conditions for (22) v and $\partial v/\partial n$ are provided (i.e. this equation is overprescribed on the boundary) while there are no boundary conditions at all for (21) (i.e. this equation can have many solutions). Equations (21) and (22) form a coupled pair of BIEs for the variables u and $\partial u/\partial n$ and they must be solved simultaneously. A biharmonic problem with the prescribed boundary conditions v and $\partial v/\partial n$ is seen to provide a good means of testing and validating numerical methods.

It is known that the order of continuity of the dependent variables required by the inverse statement (BIEM) is less than that required by the weak form (FEM) and the strong form (FDM). In BIEMs, the dependent variables along the boundary are required to be square integrable (i.e. they are allowed to be discontinuous at discrete points but finite throughout the region) [14]. Numerical results will show that any small oscillations in the computed boundary solution u greatly affect the accuracy of the overall boundary solutions. For the case of smooth geometries, the non-iterative coupled approach can be applied directly. However, special care needs to be paid to the case of non-smooth geometries. For some test problems, it is found that the use of iterative decoupled approach to generate a computational boundary condition for u is necessary in order to prevent large fluctuations in the computed boundary solutions.

5.2.1 Example 4: BTP, BC2, circular domain (smooth geometry)

The benchmark test problem is considered again, but with a circular domain of radius R. To avoid the transfinite diameter geometry $R = 1$ for which the boundary integral equations (4) and (5) might not have a unique solution [9,35], the radius is chosen to be $R = 2$.

The boundary is equally divided into two segments. A number of uniform discretizations

$(15\times 2, 20\times 2, \cdots, 40\times 2)$ and a test set of 50×2 points are employed along the boundary. The coupled approach is employed, where two coupled equations (21)-(22) are solved simultaneously for the whole set of variables $\{u, \partial u/\partial n\}$. Again, the IRBFN boundary results are more accurate than the linear and quadratic ones by several orders of magnitude as displayed in Figures 2. Figure 3 presents an enlargement of the computed solutions at some region on the boundary. It should be pointed out that the linear case performs better than the quadratic case. The reason could be that the boundary solution u obtained by the quadratic-BIEM is less smooth than that obtained by the linear-BIEM (only C_0 continuity provided here for the boundary quantity u between elements as noted earlier), resulting in larger fluctuations in the boundary solution $\partial u/\partial n$ for the former (Figure 3). The boundary solutions converges apparently as $O(\bar{s}^{1.78})$, $O(\bar{s}^{1.15})$ and $O(\bar{s}^{2.43})$ for linear-, quadratic- and IRBFN-BIEMs, respectively. In this case, increasing the order of polynomial interpolation leads to a decrease in accuracy. In general, the use of high order Lagrange schemes needs to be cautious.

Although the boundary solutions obtained by the quadratic-BIEM are less accurate than those obtained by the linear-BIEM, the former performs better than the latter in the computation of internal solutions. For example, using the mesh of 40 boundary nodes, the error norms of the solution u computed at 80 uniformly distributed interior points are $2.0e-2$, $3.3e-3$ and $3.1e-4$ for linear-, quadratic- and IRBFN-BIEMs, respectively. It appears that spurious oscillations in the computed quadratic-BIEM solutions may cancel together during the process of evaluating integrals along the boundary.

5.2.2 Example 5: BTP, BC2, rectangular domain (non-smooth geometry)

So far, in dealing with BC2, the proposed method has been verified in a smooth geometry that gives rise to no new difficulties. The case of a non-smooth geometry involving corners is further studied here. The benchmark test problem is considered again, with the domain

of interest being a square of dimension $[-2,2] \times [-2,2]$. The boundary is divided into four segments. A number of uniform boundary discretizations, $7 \times 4, 11 \times 4, 17 \times 4, 21 \times 4$ and 27×4, are employed.

The problem is first solved by the coupled approach. To describe derivative boundary conditions at a corner, two nodes which meet at the corner are shifted inside the two segments/elements [36]. The condition numbers of the final systems of equations are from $1.49e4$ to $1.10e6$ for the above range of discretizations. Figure 4 presents the variations of the computed solutions u and $\partial u/\partial n$ along the boundary including corner regions $(s = 0, s = 4, s = 8, s = 16)$. Due to the effect of corners, large oscillations appear especially for linear and quadratic cases.

It is instructive to note that all BIE methods yield accurate internal solutions despite fluctuations in the boundary solutions. For example, at the discretization of 27×27 (i.e. 27×4 boundary nodes and 25×25 interior nodes), the error norms of the internal solution v are 0.0054, $3.30e-4$ and $1.11e-5$ for linear-, quadratic- and IRBFN-BIEMs, respectively. It appears that the evaluation of integrals along the boundary cancels out spurious oscillations.

From Figure 4, it can be seen that a small amount of noise in the boundary solution u corresponds to large noise in the boundary solution $\partial u/\partial n$. Any improvement in the approximation of u is expected to result in a great improvement in the boundary solution $\partial u/\partial n$. Based on this observation, the present work will attempt to employ an alternative way of obtaining the boundary solution u. This boundary condition is generated through an iterative process in which two equations are solved separately at each iteration (the decoupled approach) rather than directly solving the coupled system of equations for the whole set of variables as previously used (the coupled approach). The process is as follows

1. Initialize the boundary conditions for u and $\partial u/\partial n$;

2. Compute the internal solutions $\partial v/\partial x$ and $\partial v/\partial y$ by carrying out derivatives on the BIE (5) for interior points;

3. Differentiate the results obtained from the previous step using linear, quadratic or IRBFN approximation in order to update the boundary condition for u according to

$$u = \frac{\partial^2 v}{\partial x^2} + \frac{\partial^2 v}{\partial y^2};$$

4. Solve the BIE (21) to update the boundary condition for $\partial u/\partial n$;

5. Check for convergence;

6. If not yet converged, repeat from step 2

7. If converged, stop.

The exact value of the function u at four corners can be found using the prescribed boundary conditions. These values are utilized during the iterative process. For all methods, the solutions are significantly improved (Figure 5). In the case of quadratic-BIEM, the boundary solutions converge as $O(\bar{s}^{0.2473})$ and $O(\bar{s}^{0.8664})$ for the coupled and decoupled approaches, respectively; at the finest mesh, their error norms are 10.4216 and 0.0464. In the case of IRBFN-BIEM, the corresponding values are $O(\bar{s}^{0.4199})$, $O(\bar{s}^{1.2387})$, 0.1662 and 0.0052. Regarding matrix rank, the decoupled approach yields considerably better condition numbers of the system matrices than the coupled approach; the condition numbers of the IRBFN-BIEM are from 33.95 to 142.66 for the range of discretizationes used. Results for the internal solutions are presented in Table 2. The proposed method attains greater accuracy than the quadratic-BIEM. Fast convergence rates are obtained for both IRBFN- and quadratic-BIEMs. In this test case, the decoupled approach is far superior to the coupled approach. In other words, by iteratively generating a computational boundary condition for u, one can avoid spurious oscillatory behaviour in the computed boundary solutions.

5.2.3 Example 6: a clamped rectangular plate under a central load

The bending of a rectangular plate with clamped edges under a concentrated load F at the centre is analyzed here. In contrast to the previous example, all boundary data $BC2$ are zero. The governing integral equations (21)-(22) are thus reduced to

$$\int_{\Gamma} \frac{\partial G^H(P,Q)}{\partial n} \left(u(Q) - u(P)\right) d\Gamma = \int_{\Gamma} G^H(P,Q) \frac{\partial u(Q)}{\partial n} d\Gamma$$
$$- \int_{\Omega} G^H(P,Q) p(Q) d\Omega, \tag{43}$$
$$\int_{\Gamma} \left(\frac{\partial G^B(P,Q)}{\partial n} u(Q) - G^B(P,Q) \frac{\partial u(Q)}{\partial n} \right) d\Gamma + \int_{\Omega} G^B(P,Q) p(Q) d\Omega = 0, \tag{44}$$

which involve the boundary quantities u and $\partial u/\partial n$ only. In this simple case ($BC2 = 0$), numerical results show that no fluctuations are observed in the computed boundary conditions by using the coupled approach. Both coupled and decoupled approaches yield smooth boundary solutions.

To compare with the quadratic-BIEM results using 16 quadratic elements obtained by Karami et al [7], the equivalent boundary discretization of 9×4 is employed. The decoupled approach is utilized here. Results of the dimensionless deflection at the centre v_c and the maximum dimensionless bending moment at the fixed ends u_{max} are displayed in Table 3 for various values of b/a in which a and b are the lengths of the sides. Compared with the analytical results [34], good agreement is achieved. For v_c, both numerical methods yield highly accurate results while for u_{max}, the proposed method yields greater accuracy than the quadratic-BIEM.

5.3 Numerical efficiency

Apart from the above comparison of accuracy and convergence rate, the efficiency of IRBFN- and linear-BIEMs are examined numerically in this section through the solution

of the example in section 5.2.1. All BIEM codes are written in MATLAB language (version 6.5R13 by The MathWorks, Inc.); they are run on a 999MHz Pentium PC. The present linear-BIEM program is similar to the one produced by Brebbia and Dominguez [36]. The most time-consuming part is the construction of the system matrix. It is reiterated that both methods are based on the same flow diagram and their final systems of equations have the same size. The main distinguishing feature between the two methods is that the number of elements (segments) in the IRBFN-BIEM is significantly less than that in the linear-BIEM. Hence, the loop (a FOR statement) to cover the entire boundary is much shorter with the former. By taking into account the effect of vectorization, the IRBFN-BIEM code achieves a great improvement in computational efficiency over the linear-BIEM as shown in Table 4.

6 Conclusion

This paper reports a new high order BIE method for the analysis of biharmonic problems. Unlike the conventional BIEMs, all boundary values in the governing integral equations including geometries are represented by indirect RBFNs. Prior conversions of the sets of network weights into the sets of nodal variable values are employed in order to form a square system of equations that can be solved by Gaussian elimination. For the first biharmonic Dirichlet problems with non-smooth geometries and boundary conditions of complex shapes, the iterative decoupled approach is better than the non-iterative coupled approach with regard to the capability of preventing large fluctuations in the computed boundary solutions. Numerical results show that the performance of the proposed method is far superior to that of the linear and quadratic-BIEMs.

Acknowledgements N. Mai-Duy wishes to thank the University of Sydney for a Sesqui Postdoctoral Research Fellowship. We would like to thank the referees for their helpful comments.

References

1. Jaswon MA. Maiti M. Symm GT. Numerical biharmonic analysis and some applications. International Journal of Solids and Structures 1967; 3: 309-332.

2. Bezine GP. Boundary integral formulation for plate flexure with an arbitrary boundary conditions. Mechanics Research Communications 1978; 5: 197-206.

3. Stern M. A general boundary integral formulation for the numerical solution of plates bending problems. International Journal of Solids and Structures 1979; 15: 769-782.

4. Costa JA. Brebbia CA. Plate bending problems using B.E.M. In Brebbia CA, editor. Boundary Elements VI 1984; 3/43-3/63. Berlin: Springer-Verlag.

5. Ingham DB. Kelmanson MA. Bounday Integral Equation Analyses of Singular, Potential, and Biharmonic Problems (Vol. 7). In: Brebbia CA, Orszag SA, editors. Lecture Notes in Engineering. Berlin: Springer-Verlag; 1984.

6. Paris F. De Leon S. Simply supported plates by the boundary integral equation method. International Journal for Numerical Methods in Engineering 1986; 23: 173-191.

7. Karami G. Zarrinchang J. Foroughi B. Analytic treatment of boundary integrals in direct boundary element analysis of plate bending problems. International Journal for Numerical Methods in Engineering 1994; 37, 2409-2427.

8. Lesnic D. Elliott L. Ingham DB. The boundary element solution of the Laplace and biharmonic equations subjected to noisy boundary data. International Journal for Numerical Methods in Engineering 1998; 43: 479-492.

9. Zeb A. Elliott L. Ingham DB. Lesnic D. A comparison of different methods to solve inverse biharmonic boundary value problems. International Journal for Numerical Methods in Engineering 1999; 45: 1791-1806.

10. He W-J. An equivalent boundary integral formulation for bending problem of thin plates. Computers and Structures 2000; 74: 319-322.

11. Sawaki Y. Kako A. Kitaoka D. Kamiya N. Plate bending analysis with *hr*-adaptive boundary elements. Engineering Analysis with Boundary Elements 2001; 25: 621-631.

12. Sladek J. Sladek V. Mang HA. Meshless formulations for simply supported and clamped plate problems. International Journal for Numerical Methods in Engineering 2002; 55: 359-375.

13. Banerjee PK. Butterfield R. Boundary Element Methods in Engineering Science. London: McGraw-Hill; 1981.

14. Brebbia CA. Telles JCF. Wrobel LC. Boundary Element Techniques Theory and Applications in Engineering. Berlin: Springer-Velag; 1984.

15. Telles JCF. A self-adaptive co-ordinate transformation for efficient numerical evaluation of general boundary element integrals. International Journal for Numerical Methods in Engineering 1987; 24: 959-973.

16. Press WH. Flannery BP. Teukolsky SA. Vetterling WT. Numerical Recipes in C: The Art of Scientific Computing. Cambridge: Cambridge University Press; 1988.

17. Haykin S. Neural Networks: A Comprehensive Foundation. New Jersey: Prentice-Hall; 1999.

18. Micchelli CA. Interpolation of scattered data: distance matrices and conditionally positive definite functions. Constructive Approximation 1986; 2: 11-22.

19. Park J. Sandberg IW. Universal approximation using radial basis function networks. Neural Computation 1991; 3: 246-257.

20. Park J. Sandberg IW. Approximation and radial basis function networks. Neural Computation 1993; 5: 305-316.

21. Cover TM. Geometrical and statistical properties of systems of linear inequalities with applications in pattern recognition. IEEE Transactions on Electronic Computers 1965; EC-14: 326-334.

22. Kansa EJ. Multiquadrics- A scattered data approximation scheme with applications to computational fluid-dynamics-I. Surface approximations and partial derivative estimates. Computers and Mathematics with Applications 1990; 19(8/9): 127-145.

23. Mai-Duy N. Tran-Cong T. Approximation of function and its derivatives using radial basis function network methods. Applied Mathematical Modelling 2003; 27: 197-220.

24. Mai-Duy N. Tran-Cong T. RBF interpolation of boundary values in the BEM for heat transfer problems. International Journal of Numerical Methods for Heat & Fluid Flow 2003; 13(5): 611-632.

25. Mai-Duy N. Tran-Cong T. Neural networks for BEM analysis of steady viscous flows. International Journal for Numerical Methods in Fluids 2002; 41: 743-763.

26. Mai-Duy N. Solving high order ordinary differential equations with radial basis function networks. International Journal for Numerical Methods in Engineering, in press.

27. Franke R. Scattered data interpolation: tests of some methods. Mathematics of Computation 1982; 38(157): 181-200.

28. Madych WR. Nelson SA. Multivariate interpolation and conditionally positive definite functions. Approximation Theory and its Applications 1988; 4: 77-89.

29. Madych WR. Nelson SA. Multivariate interpolation and conditionally positive definite functions, II. Mathematics of Computation 1990; 54(189): 211-230.

30. Tanaka M. Sladek V. Sladek J. Regularization techniques applied to boundary element methods. Applied Mechanics Reviews 1994; 47: 457-499.

31. Zheng R. Coleman CJ. Phan-Thien N. A boundary element approach for non-homogeneous potential problems. Computational Mechanics 1991; 7: 279-288.

32. Nowak AJ. Neves AC. The Multiple Reciprocity Boundary Element Method. Southampton: Computational Mechanics Publications; 1994.

33. Partridge PW. Brebbia CA. Wrobel LC. The Dual Reciprocity Boundary Element Method. Southampton: Computational Mechanics Publications; 1992.

34. Timoshenko S. Woinowsky-Krieger S. Theory of Plates and Shells. New York: McGraw-Hill; 1959.

35. Constanda C. On the Dirichlet problem for the two-dimensional biharmonic equation. Mathematical Methods in the Applied Sciences 1997; 20: 885-890.

36. Brebbia CA. Dominguez J. Boundary Elements: An Introductory Course. Southampton: Computational Mechanics Publications; 1992.

Table 1: Example 3: the boundary solutions using 9×4 boundary nodes.

	$\frac{\partial v}{\partial n} \times 10^{-3}$ (error %)			
Method	$(x = 25, y = 0)$	$(x = 50, y = 0)$	$(x = 75, y = 0)$	$(x = 100, y = 0)$
Analytical	-0.1146	-0.2048	-0.2613	-0.2804
IRBFN-BIEM	-0.1150(0.35%)	-0.2051(0.15%)	-0.2616(0.11%)	-0.2807(0.11%)
Linear-BIEM	-0.126 (9.95%)	-0.222 (8.40%)	-0.276 (5.63%)	-0.298 (6.28%)
	$\mathrm{D}\frac{\partial u}{\partial n} \times 10^{2}$ (error %)			
Analytical	0.1959	0.2813	0.3243	0.3376
IRBFN-BIEM	0.1961(0.10%)	0.2812(0.04%)	0.3244(0.03%)	0.3376(0.00%)
Linear-BIEM	0.2072(5.77%)	0.2828(0.53%)	0.3277(1.05%)	0.3394(0.53%)

Table 2: Example 5: the error norm of the internal solutions.

Method	7×7	11×11	17×17	21×21	27×27
			$N_e(v)$		
Quadratic	0.0965	0.0358	0.0111	0.0061	0.0029
IRBFN	0.0457	0.0075	0.0017	8.28e-4	3.66e-4
			$N_e(u)$		
Quadratic	0.0749	0.0272	0.0093	0.0055	0.0029
IRBFN	0.0182	0.0038	9.96e-4	5.31e-4	2.53e-4

Table 3: Example 6: the dimensionless deflection at the centre v_c and the maximum dimensionless bending moment at the fixed ends u_{max} using 16 quadratic elements/9×4 boundary nodes. Note that a and b are the lengths of the sides.

	v_c			u_{max}		
b/a	Quadratic	IRBFN	analytical	Quadratic	IRBFN	analytical
1.0	0.0056	0.0056	0.0056	0.1266	0.1257	0.1257
1.2	0.0065	0.0065	0.0065	0.1502	0.1492	0.1490
1.6	0.0071	0.0071	0.0071	0.1671	0.1652	0.1651
2.0	0.0073	0.0072	0.0072	0.1708	0.1675	0.1674

Table 4: Example 4: total CPU times used to obtain the boundary solutions at 100 test nodes and the internal solution at 80 uniformly distributed points.

No. of	Linear-BIEM		IRBFN-BIEM	
boundary nodes	No. of elements	Time (s)	No. of elements	Time (s)
30	30	5.8	2	0.9
40	40	8.4	2	1.1
50	50	11.4	2	1.5
60	60	14.7	2	1.9
70	70	18.3	2	2.3
80	80	22.5	2	2.8

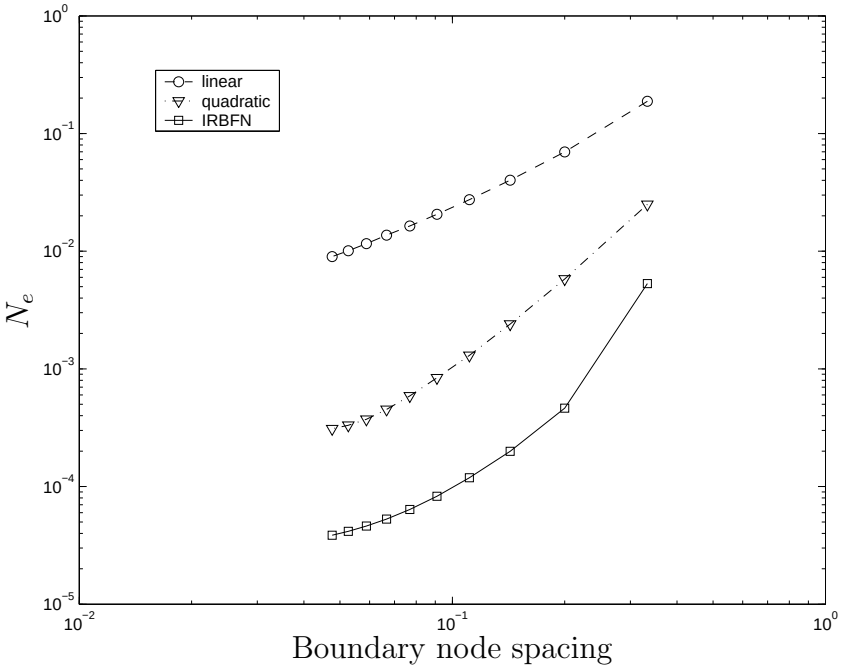

Figure 1: Example 1: accuracy and convergence rate.

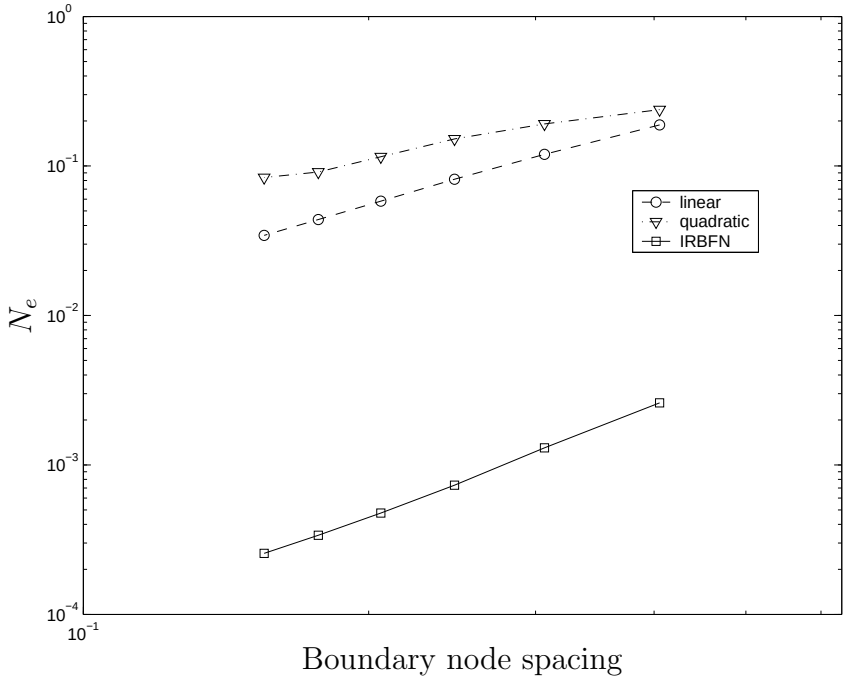

Figure 2: Example 4: accuracy and convergence rate.

a) Linear

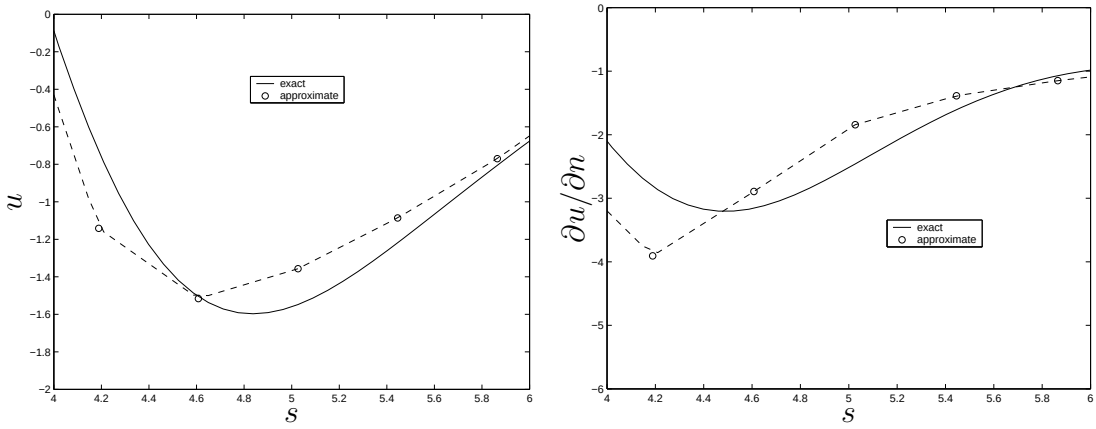

b) Quadratic

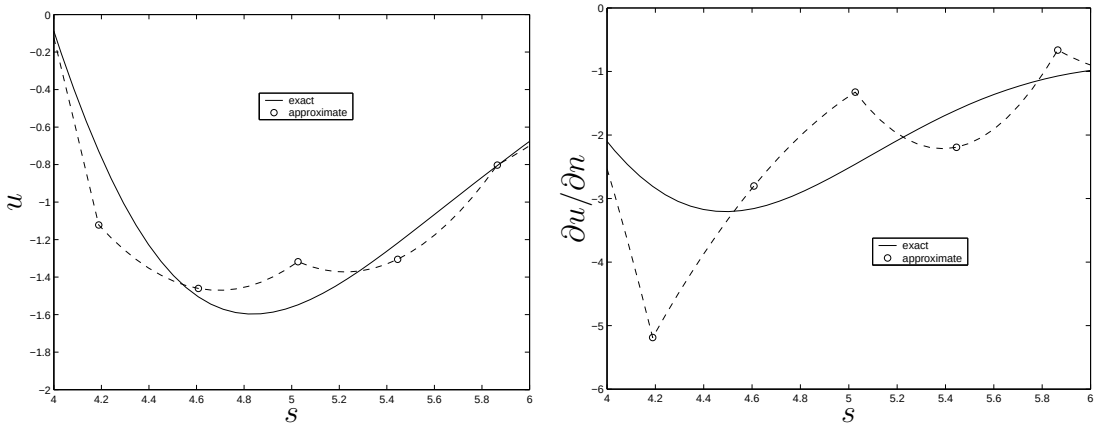

c) IRBFN

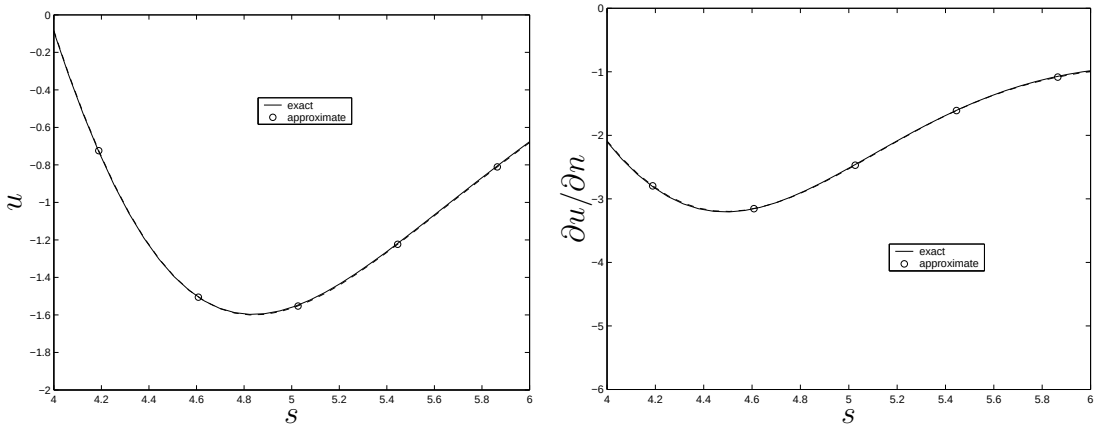

Figure 3: Example 4, 15×2 boundary nodes: zoom in on the computed boundary solutions u and $\partial u/\partial n$.

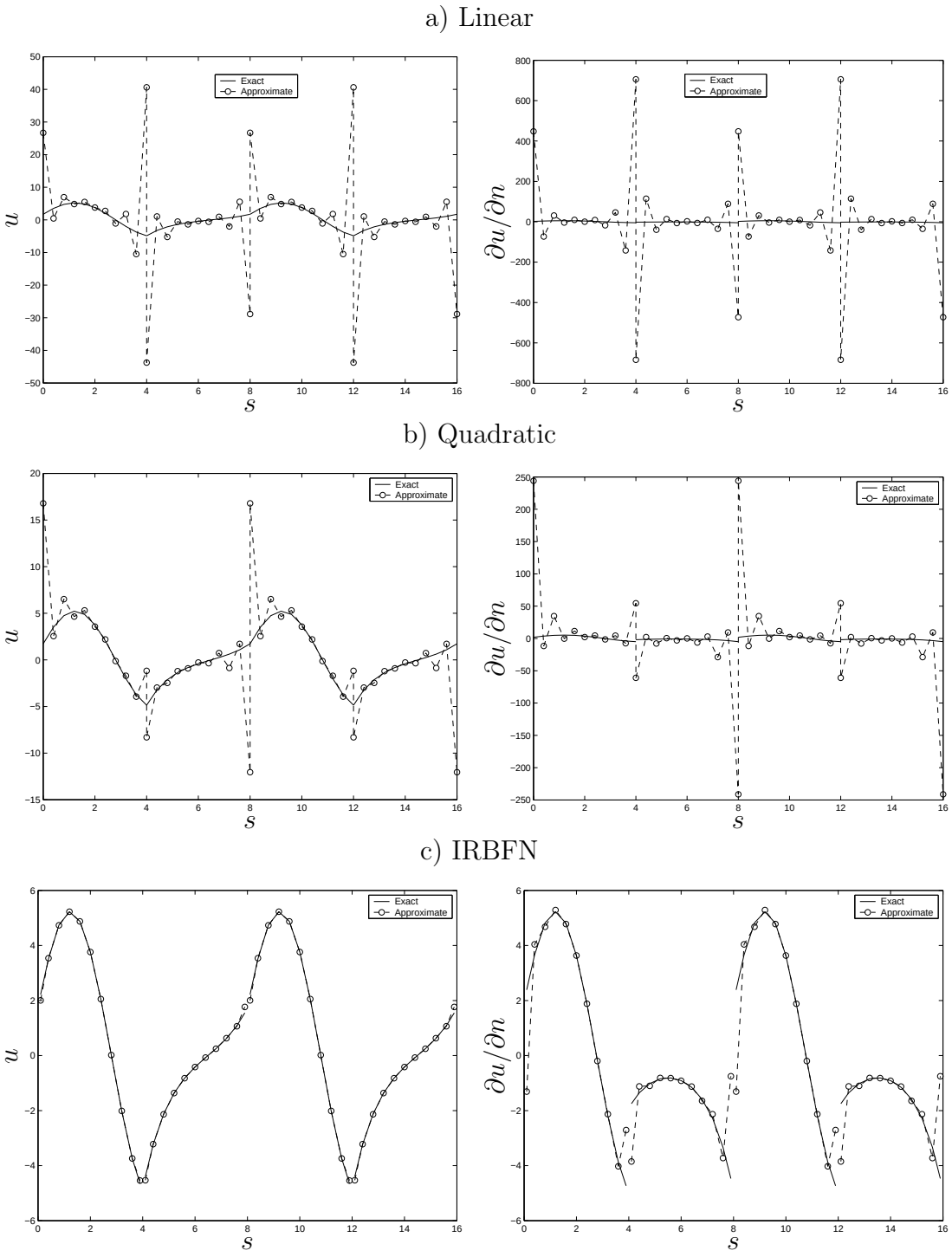

Figure 4: Example 5, 11×4 boundary nodes: effect of the corner on the boundary solutions in the case of using non-iterative coupled approach.

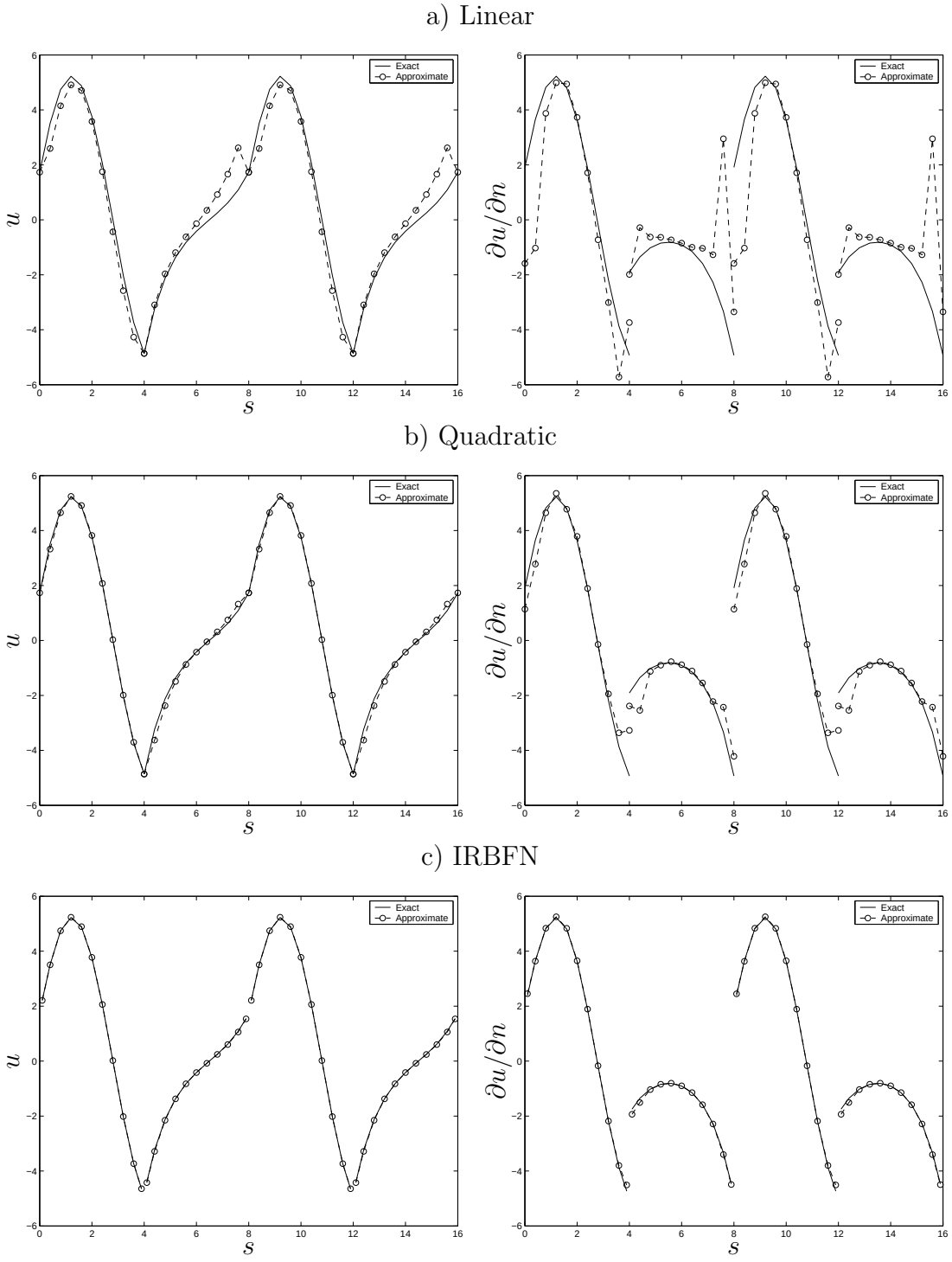

Figure 5: Example 5, 11×4 boundary nodes: effect of the corner on the boundary solutions in the case of using iterative decoupled approach.